Available online at www.sciencedirect.com
ScienceDirect
Microelectronic Engineering 85 (2008) 355–364
MICROELECTRONIC ENGINEERING
www.elsevier.com/locate/mee

Deep reactive ion etching (Deep-RIE) process for fabrication of ordered structural metal oxide thin films by the liquid phase infiltration method

Minoru Mizuhata *, Takuya Miyake, Yuki Nomoto, Shigehito Deki

Department of Chemical Science and Engineering, Graduate School of Engineering, Kobe University, 1-1 Rokkodai-cho, Nada, Kobe 657-8501, Japan

Received 18 June 2007; accepted 17 July 2007
Available online 24 July 2007

Abstract

Deep reactive ion etching (Deep-RIE) process was established for fabrication of highly nano-ordered metal oxide thin films such as TiO_2, ZrO_2, SnO_2 etc, by the liquid phase infiltration (LPI) method. Electron beam lithography (EBL) technique and Deep-RIE were adapted to fabricate the Si wafer coated with a positive resist ZEP520A. Etching gas of SF_6 and C_4F_8 was used for Deep-RIE process. The flow rate and repeating time were optimized in order to obtain the straight shape on the sidewalls of the trench or pillar structure. We used polymethylmethacrylate (PMMA) and acetylcellulose as a replica films. The transcribed replica films are applied to the liquid phase deposition reaction. The film structure was completely reproduced from the original shape of the designed Si wafer. The optical interference on the fabricated metal oxide thin films was also observed using absolute reflective visible spectroscopy.

Keywords: Deep-RIE; Electron beam lithography; ZEP520A; Sulfur hexafluoride; Octafluorocyclobutane; Liquid phase deposition process; Liquid phase infiltration method; Anatase TiO_2; SnO_2; ZrO_2

1. Introduction

In recent years, nano-ordered materials have attracted much attention since the products have been smaller in keeping with a trend of density growth or integration in various technology fields. They have great interest because of their potential to exhibit novel properties which cannot be achieved by bulk materials. For examples, two-(2D) and three-dimensionally (3D) ordered materials have attracted much interest due to their potential applications in photonic crystals [1–4], data storage [5–8], field emission device [9–12]. It is important to establish fabrication techniques of materials with desired shape or size depending on each application. For example, they must have periodic pillar or hole structures with high aspect ratio to use as 2D photonic crystals [10,11]. It is necessary to be motheye structure for use as antireflection coating [12,13], which have pointed top preferably for field emission device.

For these purposes, various methods to fabricate 2D nanostructured metal oxide have been developed. For example, highly ordered hole structured Al_2O_3 has been prepared by the anodic oxidation process [14,15]. Various kinds of oxides such as TiO_2, SnO_2 and Fe_3O_4 with micropatterned surface have been prepared by using a seed layer process [16–18]. On the other hand, a combination process of electron beam lithography (EBL) and deep reactive ion etching (Deep-RIE) techniques; so-called "Bosch Process" are adopted to LIGA process which was applied to fabricate micro- or nano-patterned materials on resist film [19–23]. In order to apply these techniques, it is easy to fabricate nanostructured Si wafer using etching gas plasma. However in case of metal oxides, they are brittle that it is not suitable for direct machining.

We have recently developed and promoted the liquid phase deposition (LPD) method as a novel aqueous

* Corresponding author. Tel./fax: +81 78 803 6186.
E-mail address: mizuhata@kobe-u.ac.jp (M. Mizuhata).

0167-9317/$ - see front matter © 2007 Elsevier B.V. All rights reserved.
doi:10.1016/j.mee.2007.07.006

solution-based process to prepare metal oxide thin films using the ligand-exchange hydrolysis of metal fluoro-complexes and the F^- consumption reaction with boric acid or aluminum metal [24]. The deposition mechanism of the metal oxides in aqueous solution is indicated by the following ligand-exchange (hydrolysis) equilibrium reaction;

$$MF_x^{(x-2n)} + nH_2O = MO_n + xF^- + 2nH^+ \quad (1)$$

The equilibrium of Eq. (1) shifts to the right-hand side upon the addition of boric acid or aluminum metal which readily reacts with F^- ions to form more stable complex ions.

$$H_3BO_3 + 4HF \rightarrow BF_4^- + H_3O^+ + 2H_2O \quad (2a)$$

$$Al + 6HF \rightarrow H_3AlF_6(Al \rightarrow Al) + 3/2\ H_2 \quad (2b)$$

The addition of boric acid or aluminum metal accelerates the ligand-exchange hydrolysis reaction. Thin films are slowly deposited on the substrate at room temperature. We have adapted LPD to the fabrication of non-SiO_2 films, such as titanium oxide [24,25], vanadium oxide [26,27], iron oxyhydroxide [28,29], and multi-component metal oxide films [30,31]. Using a simple method, it is possible to deposit on substrates with complex morphologies such as glass wool or porous materials [32]. One of the advantage of the liquid phase deposition is that metal oxide thin films were deposited into the nano-ordered restricted space among the heterogeneous phase [33,34]. Homogeneous and/or composite thin films or multi-component thin film can be also formed only by the mixing of the objective metal ions to the treatment. It is, moreover, applied to various kinds of substrates with large surface area or complex morphologies and especially nanospace as the ''Liquid Phase Infiltration Process'' [35,36]. It suggests that the LPD method can be applied to preparation of metal oxide thin films with highly ordered nanostructures.

We have been developed various kinds of LPI method, however, in this study, we focused to design the nanostructured Si as template by using EBL and Deep-RIE in order to fabricate nanostructured metal oxides. The Si structure transcribes polymer film and metal oxides are deposited on the polymer film by using LPI method and polymer film is removed. We discussed the possibility of the fabrication process of various ordered structured metal oxide thin films using various methods including the LPI process.

2. Experimental

2.1. Preparation of Si template

A p-type single crystal silicon wafer having a thickness of 525 ± 25 μm and resistivity of 5–15 Ω cm (Umesato Electronic Co., Ltd) was used. At first, high resolution positive electron beam resist ZEP520A (Nippon Zeon Co. Ltd.) was used and coated on the surface of the Si wafer by the spin coat process [37]. Spin rotation rate was 200 rpm for 5 s and subsequently 3000 rpm for 120 s. Film thickness was controlled at 400 nm. Resist-coated Si wafer was baked at 180 °C for 3 min. An electron beam lithography system Elionix ELS-3700 was utilized in order to draw a nano-order pattern on the wafer. An acceleration voltage and beam current were 30 kV and 1 pA, respectively. Dose time of the electron was 0.2 s and 0.3 s for piller-type designed wafer and trench-type designed wafer, respectively. After e-beam process, the wafer was immersed into *o*-xylene (Nacalai Tesque Inc.) as a developer solution at 23 °C with 0.1 K of error range for 50 s after selective exposure to a light source. Finally, the etching process was carried out by ICP dry etching method by Elionix EIS-700. SF_6 plasma was used as the etching step, and C_4F_8 and O_2 plasma were used as the overcoating deposition step. Power for ICP was 500 W and power for plate was 30 W and 0 W for SF_6 and C_4F_8 gas plasma irradiation, respectively.

2.2. Preparation of polymer template

In this study, polymethylmethacrylate (PMMA) and acetylcellulose was used for replication of Si morphology. Since polymethylmethacrylate (PMMA) is thermoplastic resin with low glass transition temperature, it is easy and inexpensive to cast and synthesize the template materials imprinted from the substrate. In order to fabricate polymer template, PMMA prepared by bulk polymerization method was employed. Eighty grams of methylmethacrylate monomer (MMA; Nakarai Tesque Inc.) and 1.5 g of azobisisobutyronitrile (AIBN; Nacalai Tesque Inc.) were mixed in the reactor at 80 °C under N_2 atmosphere for 8 or 28 min to obtain optimum polymer for imprinting. After polymerization reaction period, chloroform and methanol were added into the reactor sequentially. In this paper, PMMA-8 and PMMA-28 denote the ones of which polymerization times were 8 and 28 min, respectively.

On the other hand, acetylcellulose was used for preparation of the trench structured sample for the measurement of absolute refractive spectra. The acetylcellulose sheet was pressed on the Si substrate on which methylacetate was applied for swelling.

2.3. Preparation of tin fluorocomplex solution for LPD reaction

As a parent solution, Tin fluoride (SnF_2; Nacalai Tesque Inc.) was dissolved in distilled water. $SnO_2 \cdot nH_2O$ was precipitated by oxidation of fluoric solution upon addition of hydrogen peroxide (H_2O_2; Santoku Chemical Inc.). After filtration of the precipitate, it was washed with distilled water repeatedly and dried at ambient temperature. Then the precipitation was dissolved in aqueous hydrofluoric acid (HF 55%, Stella Chemifa Inc.) solution at concentration of 1.5 mol dm^{-3}, and it was used as the parent solution. Finally, the concentrations of SnO_2-HF and H_3BO_3 in the reaction solution were controlled to 0.024 mol dm^{-3}

and 0.2 mol dm^{-3} in which transparent films can be obtained.

2.4. Preparation of titanium fluorocomplex solution for LPD reaction

As a parent solution, ammonium hexafluorotitanate; $(NH_4)_2TiF_6$ (Morita Chemical Industries Co. Ltd.), and boric acid, H_3BO_3 (Nacalai Tesque Inc.), were separately dissolved in ion-exchanged water to give concentration of 0.5 mol dm^{-3}. These solutions were then mixed together and used as the treatment solution. Final concentration of $(NH_4)_2TiF_6$ and H_3BO_3 in the reaction solution were 0.1 mol dm^{-3} and 0.2 mol dm^{-3}, i.e. in the concentration range where transparent films can be obtained [24,25].

2.5. Preparation of zirconium fluorocomplex solution for LPD solution

As a parent solution, hexafluorozirconate acid (H_2ZrF_6) solution (Hashimoto Chemical Corp.) was diluted by distilled water at the concentration of 0.278 mol dm^{-3}, and prepared the treatment solution [38]. Al metal plate, of which purity is 99.98%, was added as the F^- scavenger. Final concentration of H_2ZrF_6 in the reaction solution was 0.06 mol dm^{-3}.

2.6. Fabrication of metal oxide with highly ordered periodic structure

In order to deposite the hydrophobic thin layer on the Si template, C_4F_8 plasma gas was exposed on the Si template by the ICP dry etcher at final procedure of Deep-RIE process. It is important to transcribe the Si template on PMMA, these conditions are the coil power = 500 W and the flow rate of C_4F_8 = 50 sccm for 3 min. PMMA was placed on the Si template and pressed against the Si mold at 150 °C. After 10 s, the PMMA was cooled and peeled off and used as substrate for LPD reaction.

For the substrate, both Si wafer and transcribed PMMA and acetylcellulose were used. The substrate was suspended in the LPD reaction solution vertically. After several hours, the substrates were removed from the solution and washed with distilled water. The samples were dried at room temperature. The Aron Ceramic (Toa Gosei, Ltd.) was applied to the top surface of the SnO_2 to be supported. For the PMMA subsltrate, the PMMA was immersed in acetone and methanol (v/v = 1:1) for 5 min, revealing the SnO_2 film and a positive PMMA image of Si mold. As the optimum condition depends on the nano- or micropatterns of Si wafer, each condition is described below.

For measurement of reflective spectra, acetylcellulose replica film was used. The nickel backing layer was applied on the opposite side of the acetylcellulose film. Nickel film was applied by electroless plating method using nickel sulfate solution and supported by Aron Ceramics.

2.7. Characterization of fabricated Si wafers and metal oxide

The surface morphology of fabricated Si wafers, PMMA and prepared metal oxide thin films with highly ordered periodic structure were observed by field emission scanning electron microscopy JEOL JEM-6335F. To prevent the surface of samples from electron charging up, thin carbon film was coated on the samples using carbon coater CC-40F (Meiwafosis Co. Ltd.). EDX elemental mapping analyzer JEOL EX-23000BU was used to elucidate the deposition of fluorocarbon on the surface of fabricated Si mold. To prevent the surface of samples from electron charging up, thin carbon film was coated on the samples using carbon coater. The glass transition temperature (T_g) of all the PMMA was determined by differential scanning calorimetry (DSC). DSC measurements were performed using a Thermo plus DSC 8230L (Rigaku Denki Co.) with a heating rate of 10 K/min in air atmosphere.

Visible interference spectra of transcribed trench structured TiO_2 thin films deposited on acetylcellulose template were measured by JASCO UV–Vis spectrometer V-7200 with absolute reflective attachment VAR-7020. The measured wavelength range was from 350 to 800 nm at various incident angles for the reflective spectra measurement. The incident angle ranged from 10 to 60°.

3. Results and discussion

3.1. Optimal gas flow for Deep-RIE method

For the preparation of the template substrate for the solution process such as the liquid phase deposition, it is necessary to consider the linearity of the side wall of each pillar and trench structure for keeping good liftoff condition of the oxide from the substrate. Especially, the opening part should be avoided an acute angle with sidewall and top surfaces. Etching conditions depend on the equipment, the substrate, mask, gases and so on [19–23,39–44]. Fig. 1. shows the etched profiles and recipes of adjusting the SF_6 gas. In this case, the cycle numbers of the gas flow of SF_6 and C_4F_8 was five in order to take a certain aspect values for the observation of morphology. Comparing among the results of Fig. 1a–c, in which flow times were same, the scallop on the Si pillar becomes increasingly prominent as the flow rate increased. Even the product values of [flow rate (sccm) × flow time (s)] are constant, the same results were observed, as the flow rate increased; the flow times decreased in single cycle. It is important for fabrication of Si template having various structures to decide the condition.

In order to investigate the optimum condition to have a smooth sidewall surface and a high aspect ratio structure, parametric study was performed including SF_6 gas flow rate, C_4F_8 flow rate, flow time and etching cycle times. At first, supposing that all the SF_6 gas flowing into the chamber is involved etching process, optimum condition was investigated by changing the product value; [flow rate

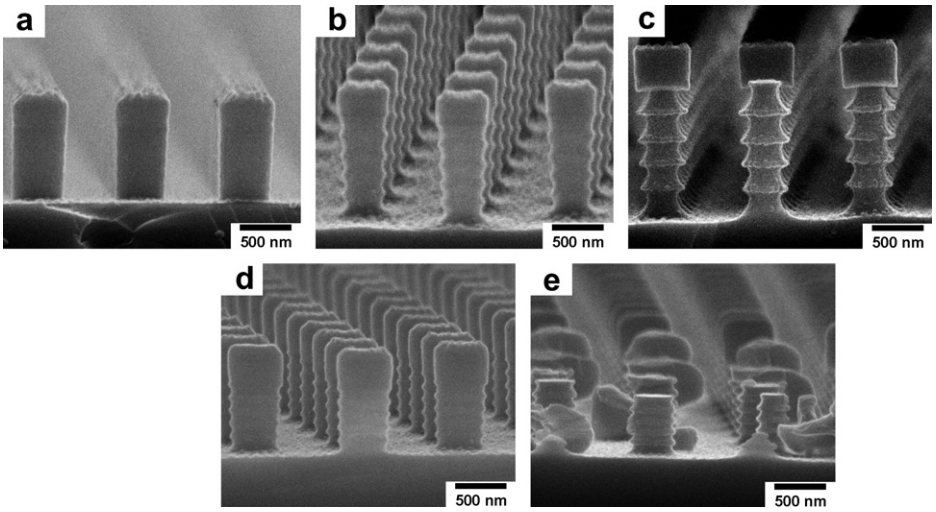

Fig. 1. Surface morphology of etched Si wafer by EBL and Deep-RIE process after 5 cycle. SF_6 gas flow rate and flow time for each operation: (a) 4 sccm, 10 s, (b) 6 sccm, 10 s, (c) 10 sccm, 10 s, (d) 6.7 sccm, 6 s, and (e) 10 sccm, 4 s. C_4F_8 gas flow rate and flow time for each operation: 15 sccm, 10 s.

(sccm) × flow time (s)] of SF_6 in range of 40–100 and 3 types of condition were tried on. In this case, the C_4F_8, plasma power, chamber temperature and pressure were kept at constant condition as shown in Fig. 1. Judging from the results so far obtained, flow rate of SF_6 gas should be used within 6 sccm.

Secondary, as in the case of the condition in constant SF_6 flow, the product values of [flow rate (sccm) × flow time (s)] of C_4F_8 was changed in range of 100–300 and 3 types of condition were tried on. Figs. 2 and 3. show the dependence of the flow rate and flow time on the surface morphology on various SF_6 and C_4F_8 supplying condition for the pillar and trench designed Si wafers based on the above results. For both cases, while etching rate increased, the scallop on the Si pillar became increasingly prominent as the product values of [flow rate (sccm) × flow time (s)] of SF_6 increases. On the other hand, etching rate decreases and the scallop on the Si pillar becomes smaller as the

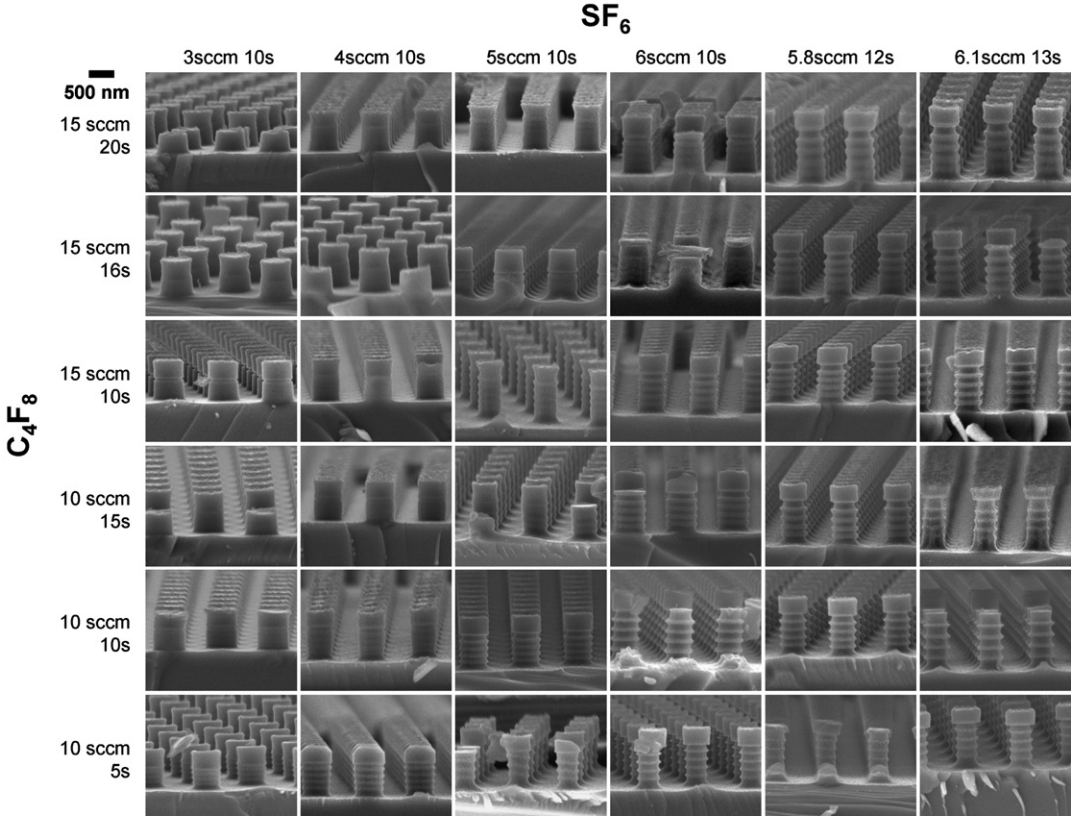

Fig. 2. Dependence of C_4F_8 and SF_6 flow condition on surface morphology of pillar-structured Si wafer.

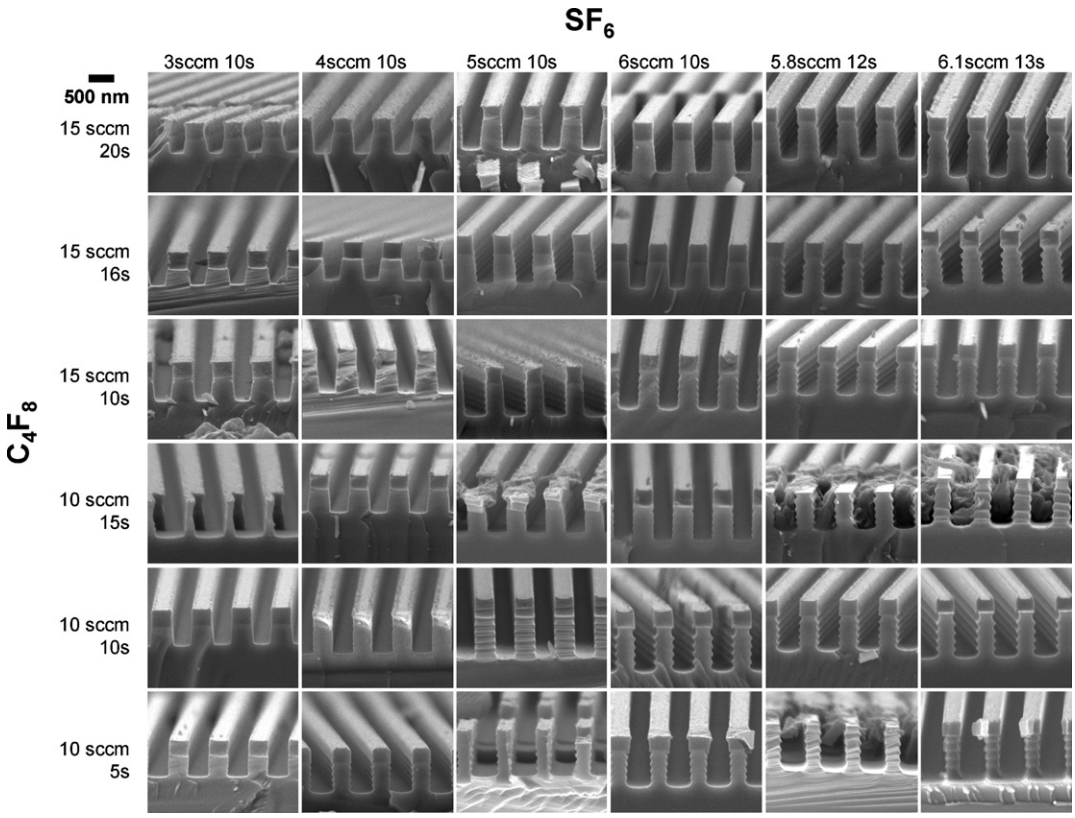

Fig. 3. Dependence of C_4F_8 and SF_6 flow condition on surface morphology of trench-structured Si wafer.

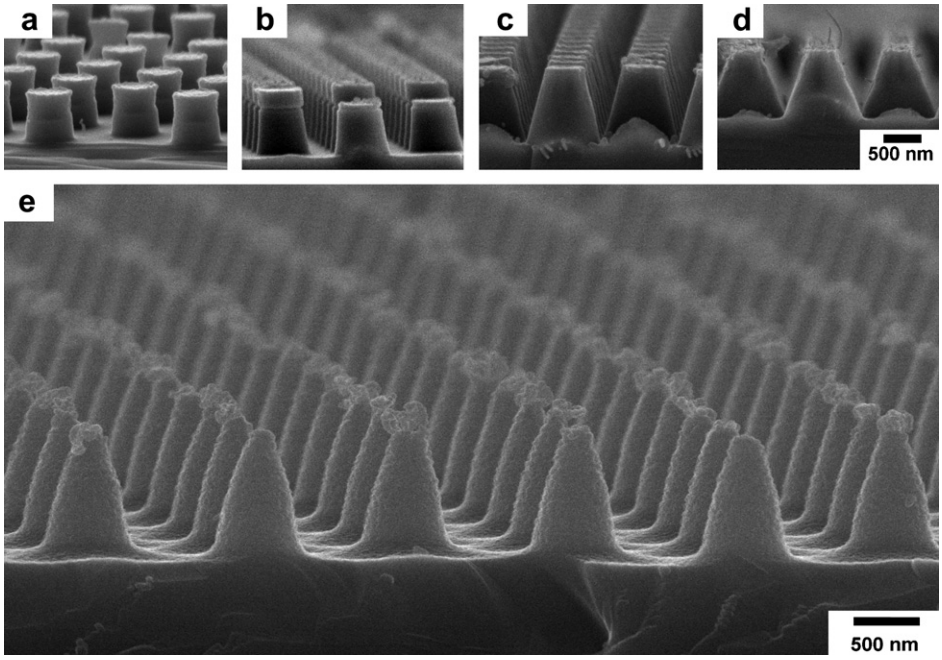

Fig. 4. Variation of surface morphology of Si wafer into motheye structure with the etching cycle numbers of SF_6 and C_4F_8 gas flow. Etching cycle number: (a) 5, (b) 10, (c) 20, (d) 25, and (e) 28 cycles. SF_6 gas flow: 4 sccm and 7.5 s, C_4F_8 gas flow : 10 sccm and 25 s.

product values of [flow rate (sccm) × flow time (s)] of SF_6 decreases. In C_4F_8, etching rate increases and the scallop on the Si pillar becomes smaller as the product values of [flow rate (sccm) × flow time (s)] of C_4F_8 increases. Therefore the scallop on the Si pillar is hardly seen, optimum condition was set as preparing Si pillar under the following condition; SF_6 flow rate = 4 sccm, flow time 10 s and C_4F_8 flow rate = 10 sccm, flow time 15 s.

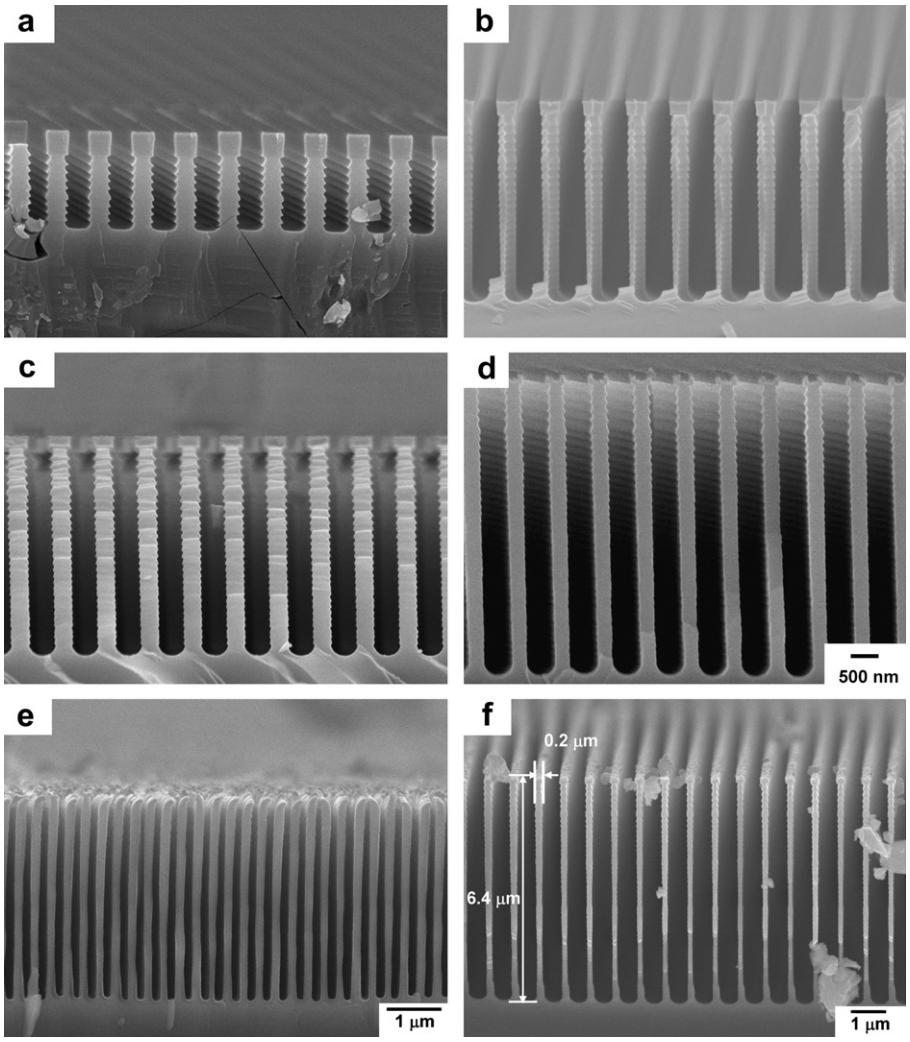

Fig. 5. Variation of surface morphology of Si wafer into deep trench structure with etching cycle numbers of SF_6 and C_4F_8 gas flow. Etching cycle number: (a) 10, (b) 20, (c) 30, (d) 40, (e) 40, and (f) 50. SF_6 gas flow: (a–d) 10 sccm and 3 s, (e) 20 sccm and 4 s, (f) 6 sccm and 4 s. C_4F_8 gas flow : (a–d) 15 sccm and 16 s; (e, f) 50 sccm and 5 s.

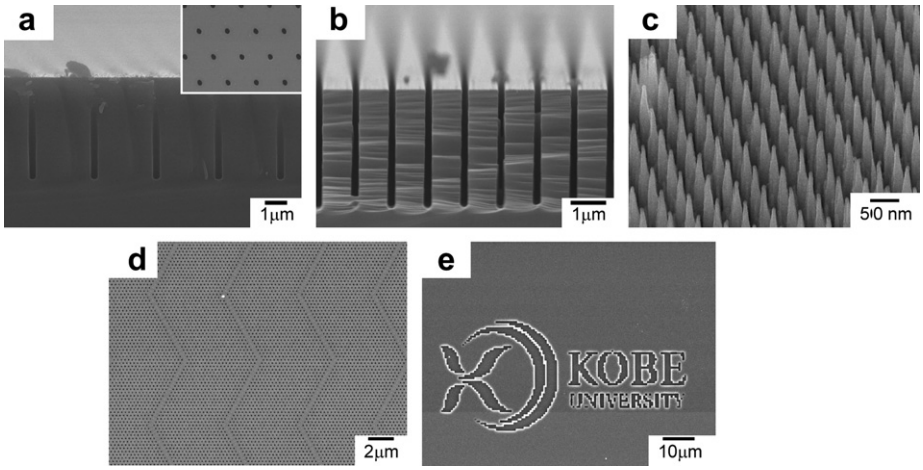

Fig. 6. Various Si templates prepared by Deep-RIE process. SF_6 gas flow: 20 sccm and 4 s. C_4F_8 gas flow: 50 sccm and 5 s.

3.2. Fabrication of Si substrate with various structures

Variation of surface morphology of Si wafer into moth-eye structure with the etching cycle number of SF_6 and C_4F_8 gas flow is shown in Fig. 4. In this case, each value of gas flow rate and time was larger than that for pillar structure indicated in Fig. 2.; SF_6 gas flow rate and time are 4 sccm and 7.5 s, and C_4F_8 gas flow rate and time are 10 sccm and 25 s. As increasing number of etching times, the Si substrate is etched not depth direction, but side direction. It is considered that generated F radical in chamber attacks the edge of resist mask than Si substrate.

We also tried to fabrication the trench structure with high aspect ratio. Variation of the structure of Si trench structure with the etching cycle number of SF_6 and C_4F_8 gas flow is shown in Fig. 5. As increasing number of etching times, the Si substrate is etched for depth direction and its aspect ratio increases up to ca 32. For the sample shown in Fig. 5e and f, SF_6 gas flow rate, C_4F_8 gas flow rate, and resist thickness are different from the other processes

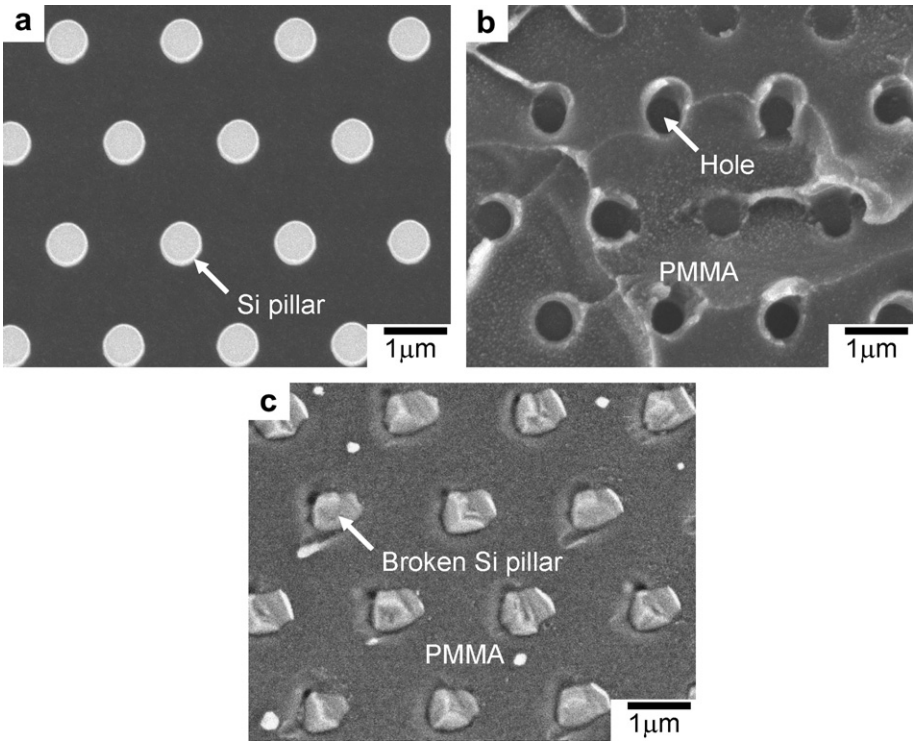

Fig. 7. SEM images of: (a) original pillared Si wafer, (b) transcribed PMMA-8 with holes transferred from Si pillars, and (c) transcribed PMMA-28 with broken Si pillars.

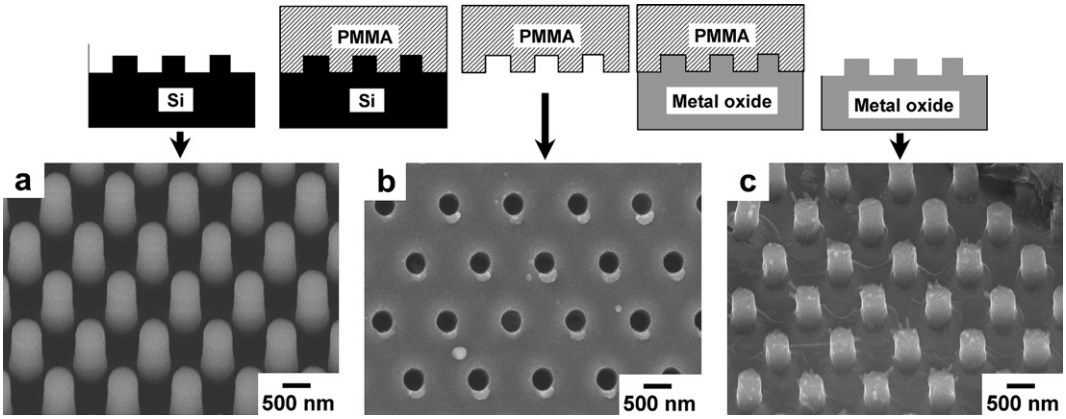

Fig. 8. SEM images of transcribing scheme: (a) periodic pillar structure of etched Si wafer, (b) transcribed PMMA-8 sample, and (c) SnO_2 depositing on PMMA template. For LPD reaction: Concentration of Sn fluorocomplex: 0.024 mol dm^{-3}, H_3BO_3: 0.2 mol dm^{-3}. Reaction time: 12 h. Temperature: 30 °C.

shown in Fig. 5a–d. The author considers that diffusion of the gas and generated F radical were different at each condition that the fabricated nanostructured Si substrates by using Deep-RIE became different structure at each condition.

As described above, specific conditions for each process were empirically found in various samples. We found that the scallop shape was easily found in most cases that SF_6 flow rate was more than 20 sccm. In Fig. 6, the SEM image of various kinds of etched Si wafer designed by the same condition. In this case, SF_6 gas flow was set in 20 sccm and 4 s and C_4F_8 gas flow was set in 50 sccm and 5 s. For all cases, there is no scallop shape and good reproducibility. To fabricate the deeply dug structure, the flow time can be short because of protect from the erosion of side wall by etching gas, although the repetition time might increased. This condition was extended to not only periodic structural design but also any drawing image such as Fig. 6e.

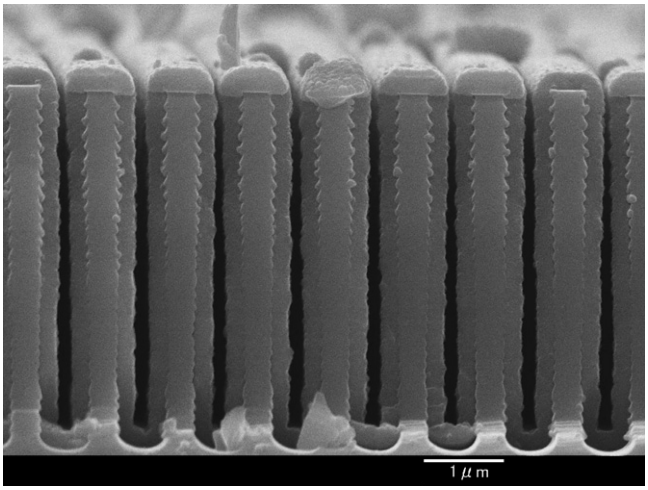

Fig. 9. SEM images of TiO_2 coated ordered structure Si wafer.

3.3. Optimum condition of PMMA for imprinting of fabricated Si pillar

According to DSC measurement of synthesized PMMA, each glass transition temperature; T_g remains within 180 °C in air condition, therefore the imprinting temperature was set 50 °C higher than each T_g. In this case, the fluorocarbon was deposited in order to improve the liftoff condition from Si surface [45]. Fig. 7. shows SEM images of Si template and PMMA transcribed the Si template. In this case, the diameter of Si pillar is 600 nm. There is no broken Si pillar rod in the PMMA-8 hole and replica form of Si template was prepared successfully as shown in Fig. 7b. However, in the case of using PMMA-28, the Si pillar rods remained in the PMMA matrix as shown in Fig. 7c. It is suggested that the shape of pillared Si wafer was transcribed into PMMA, however, the hardness of PMMA-28 caused a fail of PMMA liftoff from Si substrate. PMMA-28 has high degree of polymerization in comparison with PMMA-8, therefore its flexibility or hardness is not suitable to transcribing.

Dependence of diameter of Si pillar rod on the transcribe condition also. In the case of diameter of 400 nm,

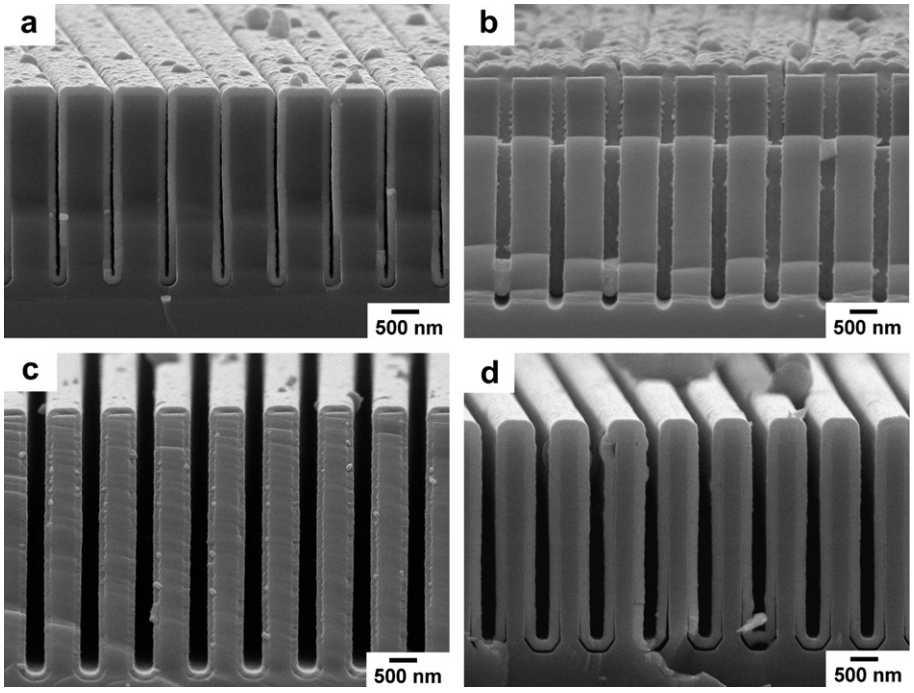

Fig. 10. SEM images of SnO_2 (a ,b) and ZrO_2 (c, d) thin films deposited on the trench structured Si wafer with high aspect ratio. Reaction time: (a) and (c) 20 h, (b) and (d) 48 h. Temperature at 30 °C.

most part of Si pillars was successfully transcribed. However, Si rod was remained in a little part of PMMA-8. In the case of diameter of 200 nm, there are small trace points made by the top of Si pillar. From these results, we tried to prepare the metal oxide thin films using Si pillar with the diameter of 500 nm and PMMA-8 as template polymer in the following experiment.

3.4. Fabrication of highly structure ordered periodic structure

Fig. 8. shows fabrication scheme of nanostructured metal oxide. Fig. 8c. shows the FE-SEM image of SnO_2 pillar array. SnO_2 exhibit hexagonal array of pillar on long length scales, with the same periodicity as the pillar on the Si substrate used as a template. Some amount of shrinkage was seen because the PMMA shrinks at heat treatment as shown in Fig. 8b. The distance and diameter were shortened by the volume change of the sample. However, its topological condition did not change during this procedure [35,36,46]. Infiltration condition was confirmed using periodic structured Si substrate. The cross section image of the TiO_2 deposited on scallop-shaped silicon pillar was shown in Fig. 9. Oxide layer is formed around the each part of Si structure with fine projection of side wall uniformly. The filling condition was enough to infiltrate among the gaps between pillar or trench structure with nano-ordered periodic structure. As well as the sample of TiO_2, ZrO_2, and SnO_2 thin films deposited on the trench structured Si substrate were shown in Fig. 10. Although deposited films was peeled off at a part of substrate due to dry-up of the oxide samples, there is no void and separation of the sample with good filling condition.

Consequently, EBL and Deep-RIE process are useful to fabricate a nanostructured template for the liquid phase deposition process.

3.5. Visible interference spectra of periodic trench structured TiO_2 thin films

Absolute refractive visible spectra of TiO_2 were shown in Fig. 11. Since the thickness of TiO_2 thin film was similar as the wavelength of visible light, the interference wave was observed for the plane thin film. Using trench structured TiO_2 thin films, intensive interference wave was observed. This wave was caused by structural condition of the periodic repetition of the TiO_2 morphology. As shown in Fig. 11 b and c, the wave shifted toward to lower wavelength, as incident angle increase, because of shortening the optical repeating distance for interference light. For each case, the interference wave eliminated at a large incident angle more than ca. 50°. It is because projective distance between trench lines became shorter than the one in which the interference phenomena.

It is suggested that the optical periodicity was established by the replication from the Si wafer by the liquid phase deposition with electronic designing.

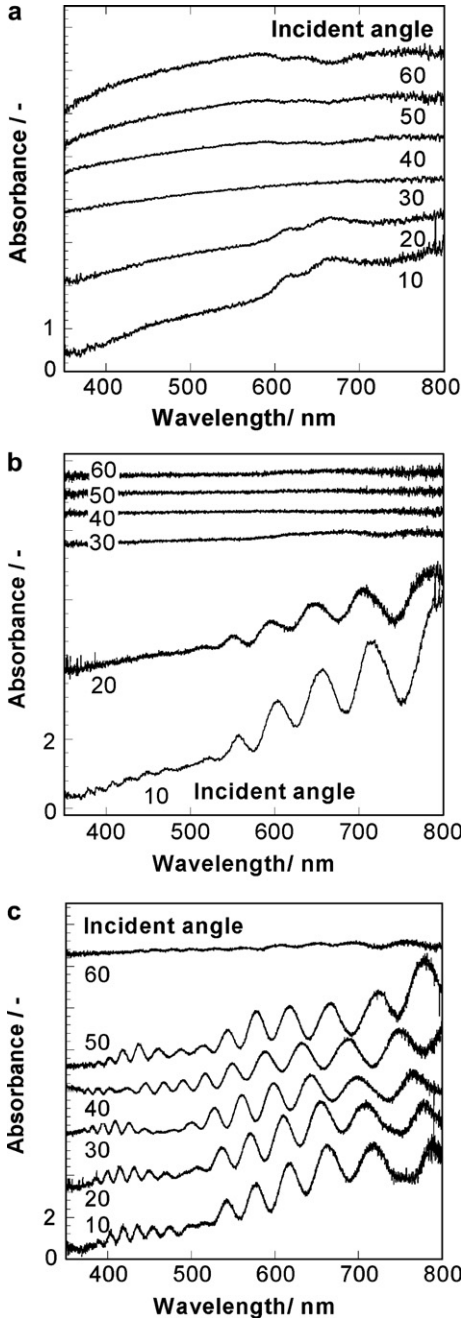

Fig. 11. Visible absolute reflective spectra of the deposited TiO_2 on periodic trench structured Si wafer. Deposition period :6 h. Surface morphology of Si substrate: (a) plane thin film, (b) pitch 500 nm and space 180 nm, (c) pitch 1000 nm and space 300 nm.

4. Conclusions

Electron beam lithography (EBL) and deep reactive ion etching (Deep-RIE) process were applied to the Si wafer coated with a positive resist for fabrication of highly nano-ordered metal oxide thin films by the liquid phase deposition method. The flow rate and repeating time were optimized in order to obtain the straight shape on the side wall of the trench or pillar structure. The productive values of [Flow rate(sccm) × flow time(s)] of SF_6 increases, the

scallop on the Si pillar becomes larger, and as the flow rate of SF_6 increases, it becomes increasingly prominent on the productive values of [Flow rate(sccm) × flow time(s)] of SF_6. We found that the scallop shape was easily found in most cases that SF_6 flow rate was more than 20 sccm. Various designed Si wafer was prepared with motheye, high aspect pillar and trench structure. We used polymethylmethacrylate (PMMA) and acetylcellulose as a replica films. By using PMMA and ceramic glue, the Liquid Phase Infiltration method found to be applied to transcribe template with various metal oxide. The structure of the oxide thin film was completely reproduced from the original shape of the designed Si wafer. The interference spectra observed by absolute reflective UV–Visible spectrometer indicated optically periodic structure.

Acknowledgments

This study was supported by Grants-in-Aid for Scientific Research (A) Nos. 15205026, 19205029 from Japan Society for the Promotion of Science and Priority Area No. 16080211 from Ministry of Education, Culture, Sports, Science and Technology of Japan.

References

[1] E. Yablonovitch, Phys. Rev. Lett. 58 (1987) 2059.
[2] V.V. Poborchii, J. Appl. Phys. 91 (2002) 3299.
[3] F. Pommereau, L. Legouezigou, G.H. Duan, B. Lombardet, J. Appl. Phys. 95 (2004) 2242.
[4] H.C. Guo, D. Nau, A. Ranke, H. Giessen, Appl. Phys. B. 81 (2005) 271.
[5] I. Soten, H. Miguez, S.M. Yang, S. Petrov, N. Coombs, N. Tetreault, N. Matsuura, H.E. Ruda, G.A. Ozin, Adv. Funct. Mater. 12 (2002) 71.
[6] T. Aoki, M. Kuwabara, Appl. Phys. Lett. 27 (2004) 2580.
[7] T. Aoki, M. Kondo, K. Kurihara, N. Kamehara, M. Kuwabara, J. Appl. Phys. 45 (2006) 350.
[8] J.E. Jang, S.N. Cha, Y. Choi, G.A.J. Ameratunga, D.J. Kang, Appl. Phys. Lett. 87 (2005) 263103.
[9] A.G. Rinzler, J.H. Hafner, P. Nikolaev, L. Lou, R.E. Smalley, Science 269 (1995) 1550.
[10] V. Mizeikis, S. Juodkazis, J.Y. Ye, A. Rode, S. Matsuo, H. Misawa, Thin Solid Films 438 (2003) 445.
[11] V.V. Poborchii, Appl. Phys. Lett. 75 (1999) 3276.
[12] H. Toyota, K. Takahara, M. Okano, T. Yotsuya, H. Kikuta, J. Appl. Phys. 40 (2001) 747.
[13] D.H. Macdonald, A. Cuevas, M.J. Kerr, C. Samundsett, D. Ruby, Solar Energ. 76 (2004) 277.
[14] H. Masuda, K. Fukuda, Science. 268 (1995) 1466.
[15] I. Mikulskas, S. Juodkazis, R. Tomasiunas, J.G. Dumas, Adv. Mater. 13 (2001) 1574.
[16] N. Shirahata, Y. Masuda, T. Yonezawa, K. Koumoto, Langmuir 18 (2002) 10379.
[17] T. Nakanishi, Y. Masuda, K. Koumoto, J. Cryst. Growth 284 (2005) 176.
[18] Y. Masuda, S. Ieda, K. Koumoto, Langmuir 19 (2003) 4415.
[19] X. Li, T. Abe, M. Esashi, Sensor Actuat. A 87 (2001) 139.
[20] Y. Chen, D. MacIntyre, S. Thoms, Microelecton. Eng. 57–58 (2001) 939.
[21] B-S. Kim, H-S. Lee, J-S. Wi, K-B. Jin, K-B. Kim, J. Jpn. Appl. Phys. 44 (2005) L95.
[22] S W. Youn, H. Goto, M. Takahashi, S. Oyama, Y. Oshinomi, K. Matsutani, R. Maeda, Microelecton. Eng., in press, doi:10.1016/j.mee.2007.05.005.
[23] H. Kawata, M. Yasuda, Y. Hirai, Microelectron. Eng. 84 (2007) 1140.
[24] S. Deki, Y. Aoi, O. Hiroi, A. Kajinami, Chem. Lett. (1996) 433.
[25] S. Deki, Y. Aoi, Y. Asaoka, A. Kajinami, M. Mizuhata, J. Mater. Chem. 7 (1997) 733.
[26] S. Deki, Y. Aoi, Y. Miyake, A. Gotoh, A. Kajinami, Mater. Res. Bull. 31 (1996) 1399.
[27] S. Deki, Y. Aoi, A. Kajinami, J. Mater. Sci. 32 (1997) 4269.
[28] S. Deki, Y. Aoi, J. Okibe, H. Yanagimoto, A. Kajinami, M. Mizuhata, J. Mater. Chem. 7 (1997) 1769.
[29] S. Deki, N. Yoshida, Y. Hiroe, K. Akamatsu, M. Mizuhata, A. Kajinami, Solid State Ion. 151 (2002) 1.
[30] S. Deki, Y. Aoi, H. Yanagimoto, K. Ishii, K. Akamatsu, M. Mizuhata, A. Kajinami, J. Mater. Chem. 6 (1996) 1879.
[31] S. Deki, H. Miki, M. Sakamoto, M. Mizuhata, Chem. Lett. 36 (2007) 518.
[32] H. Kishimoto, K. Takahama, N. Hashimoto, Y. Aoi, S. Deki, J. Mater. Chem. 8 (1998) 2019.
[33] S. Deki, A. Nakata, M. Mizuhata, Electrochemistry 72 (2004) 452.
[34] S. Iizuka, S. Ooka, A. Nakata, M. Mizuhata, S. Deki, Electrochim. Acta 51 (2005) 802.
[35] S. Deki, S. Iizuka, A. Horie, M. Mizuhata, A. Kajinami, Chem. Mater. 16 (2004) 1747.
[36] S. Deki, S. Iizuka, A. Horie, M. Mizuhata, A. Kajinami, J. Mater. Chem. 14 (2004) 3127.
[37] K. Martin, D. Brown, 2004 NNIN REU Research Accomplishments, (2004) 96.
[38] K. Kuratani, M. Uemura, M. Mizuhata, A. Kajinami, S. Deki, J. Am. Ceram. Soc. 88 (2005) 2923.
[39] Y. Chinzei, Y. Feurprior, M. Ozawa, T. Kikuchi, K. Horioka, J. Vac. Sci. Tech. A. 18 (2000) 158.
[40] A. Sankaran, M.J. Kushner, J. Appl. Phys. 97 (2005) 023307.
[41] S. Trellenkamp, J. Moers, A.V. Hurt, P. Kordos, Microelectron. Eng. 67 (2003) 376.
[42] J. Li, A.Q. Liu, Q.X. Zhang, Sensor Actuat. A 125 (2006) 494.
[43] L. Zhou, F. Luo, M. Cao, Thin Solid Film 489 (2005) 229.
[44] H.C. Liu, Y.H. Lin, W. Hsu, Microsyst. Technol. 10 (2003) 29.
[45] G.Y. Jung, Z. Li, W. Wu, Y. Chen, D.L. Olynick, S.Y. Wang, W.M. Tong, Langmuir 21 (2005) 1158.
[46] A.J. Niskanen, S. Franssila, Microelectron. Eng. 57–58 (2001) 629.